Entropy generation and thermohydraulics of mixed convection of hybrid-nanofluid in a vertical tube fitted with elliptical-cut twisted tape inserts - A computational study

Amir Mohamad Khfagi[a], Graeme Hunt[a], Manosh C Paul[a], Nader Karimi[a,b]
[a]James Watt School of Engineering, University of Glasgow, Glasgow G12 8QQ, United Kingdom
[b]School of Engineering and Materials Science, Queen Mary University of London, London E1 4NS, United Kingdom

Abstract

A numerical investigation is carried out to study the mixed convection of Al_2O_3-Cu/water hybrid-nanofluid in a vertical tube fitted with elliptical-cut twisted tape inserts (TECT). Thermodynamic irreversibilities are evaluated by calculating the Bejan number, as well as the system's local and total entropy generation. The heat transfer, friction factor, thermal performance factor, and entropy generation analyses are conducted at different volume concentrations of nanoparticles and Reynolds numbers between 7000 and 15000. The realizable k-ε model is used to simulate the turbulent, heat transferring flow computationally. The results clearly demonstrate the influence of mixed convection on heat transfer and entropy generation. In particular, mixed convection simulations predict greater Nusselt number, friction factor, and thermal performance factor than the corresponding forced convection simulations. Further, it is shown that the Nusselt number and the thermal performance factor for mixed convection are 4.6% and 5.5% higher than those forforced convection, respectively. The results also reveal that at Reynolds numbers of 7000, 9000, and 11000, the thermal entropy production dominates the total irreversibility of the system. Likewise, frictional entropy production is the dominant mode of total irreversibility in the system at high Reynolds numbers of 13000 and 15000.

Keywords: Entropy generation; Bejan number; heat transfer augmentation; turbulent mixed convection; hybrid nanofluids.

Nomenclature

a	Diameter-cut width (m)
b	Diameter-cut length (m)
Be	Bejan number (-)
$C_{1\varepsilon}, C_{2\varepsilon}, C_{3\varepsilon}, C_\mu$	Model constant
C_p	Specific heat of fluid (J Kg^{-1} K^{-1})
D	Pipe diameter (m)
f	Friction Factor
g	Gravitational acceleration (m/s^2)
G_k	Turbulent kinetic energy generation (J Kg^{-1})
G_b	Generation of turbulence Kinetic energy due to buoyancy
h	Coefficient of heat transfer (W m^{-2} K^{-1})
k	Turbulent kinetic energy (J Kg^{-1})
k_c	Fluid thermal conductivity (W m^{-1} K^{-1})
L	Tube length (m)
Nu	Nusselt number (-)
P	Pressure (Pa)
Re	Reynolds number (-)
S	Velocity strain rate tensor
S_{ij}	Linear deformation rate for a fluid element (-)
$S_{F,F}$	Frictional Entropy production (W m^{-3} K^{-1})
$S_{H,T}$	Thermal entropy production (W m^{-3} K^{-1})
$S_{g,t}$	Total entropy production (W m^{-3} K^{-1})
T	Temperature (K)
T_0	Reference Fluid temperature (K)
u	Velocity of Fluid (m s^{-1})
w	Twisted tape width (m)
y	Twisted tape pitch (m)

Greek symbols

ρ	Fluid density (Kg m^{-3})
ρ_0	Reference fluid density (Kg m^{-3})
μ	Dynamic viscosity (Pa-S)
Δp	Drop of pressure (Pa)
$\emptyset$	Solid volume fraction
η	Thermal efficiency factor (-)
σ_ε	Model constant (-)
δ	Thickness (m)
ε	Turbulent dissipation rate

Subscripts

A	Al_2O_3
C	Cu
f	Basic fluid
eff	Effective
hnf	Hybrid-nanofluid
β:	Thermal expansion coefficient
o	Reference
p	Plain tube

1 Introduction

Mixed convection flow occurs when natural (free) and forced convection mechanisms contribute comparably to heat transfer (Galvez, Loutzenhiser, Hischier, & Steinfeld, 2008). In natural convection, fluid motion is the result of fluctuating gravitational body forces and fluid density. Forced convection induces fluid mobility by the application of an external force (Bergman, Lavine, Incropera, & DeWitt, 2011). Different parameters such as flow direction, arrangement geometries and flow regimes, type of working fluid and magnitude of the temperature difference that drives heat transfer characterise the contributions of natural and forced convection (Joye, Bushinsky, & Saylor, 1989; Oni & Paul, 2015). Buoyancy forces are responsible for the formation of natural convection currents, and their direction depends on whether the forced flow is upwards, downwards, horizontal, or any mix of the three. Natural convection currents are said to be "assisting" when they move in the same direction as the forced flow, and "opposing" when they move in the opposite direction (Bergman, Lavine, et al., 2011). Several engineering applications employ mixed convection heat transfer in tubes. These include heat exchangers for cooling electrical equipment and solar collectors. Pipelines used to carry oil, and boilers are further examples (Kakaç, Shah, & Aung, 1987; Mohammed, 2008). The significance of mixed convection heat transmission in pipes has sparked various research projects in order to increase the efficiency of many industrial applications (Ozsunar, Baskaya, & Sivrioglu, 2001).

For a long time, free and forced convection were treated as independent phenomena, with little consideration given to how they may work together. Initial studies focused on laminar and transitional flow methods when looking at the possibilities of such interactions. As it comes to heat transfer in turbulent flows, buoyancy effects have lately been shown to play a significant role. Investigations of mixed convection in turbulent flow in pipes using twisted tape are uncommon in the research literature. Experiments involving mixed convection in tubes were conducted to evaluate heat transfer. Assuming a uniform heat flux and crosswise uniform wall temperatures, Barozzi et al (Barozzi, Zanchini, & Mariotti, 1985) carried out an experimental analysis of mixed convection of water with horizontal and inclined finned tubes. In this configuration, Meyer and Everts (Meyer & Everts, 2018) assessed heat transmission. A study performed by (Taher, Ahmed, Haddad, & Abid, 2021) correlated Nusselt number with Rayleigh number and Reynolds number in a horizontal pipe with uniformly heated walls. Overall the rates of heat transmission were much higher than those expected from forced convection. Overwhelmingly, mixed convection studies emphasise horizontal as well as vertical tube and duct orientation with air as the working fluid. Iqbal and Stachiewicz (Iqbal & Stachiewicz, 1966) studied the influence of flow direction at laminar mixed convection in a rising circular duct. Their findings suggested that the coefficients of heat transfer reached a maximum at the optimal flow orientation and thereafter dropped. Piva et al. (Piva, Barozzi, & Collins, 1995) analysed the mixed convection for water laminar flow over a horizontal pipe experimentally and computationally under wall uniform heat flux. Because of the buoyancy effect generated by mixed convection, the heat transmission and the pressure drops were found to rise by up to 150% and 22%, respectively. Lin and Lin (Lin & Lin, 1996) found that buoyancy improved heat transmission during an experimental study of neutrally buoyant flow, flow transition, in addition to the attendant thermal transmission mechanism in mixed convection through a channel of inclined rectangular using air as working flow. In a horizontal circular straight pipe, Ghajar (Ghajar & Tam, 1995) studied the transition zone between mixed between forced convection and mixed convection. Researchers observed that the regime map might be applied for many kinds of flows. In addition, the Prandtl number, Grashof number, and Reynolds number should be employed to take advantage of the buoyancy influence. Patil and Babu (Patil & Vijay Babu, 2012) experimented to determine the significance of non-dimensional varibles including Prandtl, Reynolds, and Richardson number for the water and ethylene glycol laminar flow of mixed convection through a plain square channel. According to this study, free convection intensity and Richardson number dropped as Reynolds number rose. As a result, mixed convection achieved a superior average Nusselt number in comparison with forced convection. At the fixed Reynolds number, a rise in the Richardson and Prandtl numbers caused the Nusselt number to rise.

For the first time, Abdelmeguid and Spalding (Abdelmeguid & Spalding, 1979) conducted numerical estimates of heat transmission and turbulent flow in vertical, horizontal, and inclination tubes

subjected to buoyancy impact under a uniform heat flux using a two-equation model. There is only a little effect of buoyancy on turbulence in low-Grashof-number locations, but in high-Grashof-number regions, it affects the average flow and heat transmission. Farouk and Ball (Farouk & Ball, 1985) computationally and experimentally evaluated the flow of mixed convection through a pipe revolving in air. They discovered that the moving cylinder's mean Nusselt number was larger than the stationary cylinders.

Some studies have used a nanofluid in mixed convection to improve heat transport. Rashidi et al. (Rashidi, Nasiri, Khezerloo, & Laraqi, 2016) devised a computational solution to study the influence of a field of magnetism on mixed convection heat transmission in a nanofluid-filled duct with the walls of sinusoidal. Mirmasoumi and Behzadmehr (Mirmasoumi & Behzadmehr, 2008) investigated the influence of nanofluid on the transport of heat in horizontal pipes by laminar mixed convection. Based on a single fluid two-phase method, a two-phase mixture model has been used to investigate fully developed mixed convection of Al_2O_3/water. In their study (Aberoumand & Jafarimoghaddam, 2016), Aberoumand and Jafarimoghaddam examined the impacts of mixed convection and nanofluids on heat transmission and stability of flow inside curved tubes. Rahmati et al. (Rahmati, Roknabadi, & Abbaszadeh, 2016) applied the lattice Boltzmann method (LBM) to create a hollow tube with a double cover and a nanofluid of Cu/water. For a cavity with a vertical wall and thermally sinusoidal heating, they evaluated mixed convection. Richardson and Nusselt numbers were found to be changing in different directions. The characteristics of a hybrid mixed convection nanofluid were studied by Qureshi et al (Qureshi, Hussain, & Sadiq, 2021) in a straight obstacle duct.

Entropy Production Minimization, as presented by Bejan (Bejan & Kestin, 1983), is a standard method for determining the quality of energy produced by a process and optimising the thermal system and its components. The Bejan number was initially suggested by Paoletti and co-workers (Paoletti, Rispoli, & Sciubba, 1989). In each convective heat transfer issue, there is a compromise between irreversibility of heat transmission and irreversibility of fluid friction (Bejan, 2013; Bejan & Kestin, 1983). Entropy generation minimization has been applied to solve free and forced convection situations with various geometry (Bejan & Lorente, 2012; Hooman, 2006; Ibáñez, Cuevas, & de Haro, 2003; Khfagi, Hunt, Paul, & Karimi, 2022; Oliveski, Macagnan, & Copetti, 2009).

Despite its importance in engineering, entropy production and heat transfer by mixed convection within turbulent flows in pipes fitted with twisted tape using hybrid-nanofluid have been largely ignored. In previous research, the effectiveness of parameters on heat transport and generation of entropy for forced convection has been investigated for pipes supplied with elliptical cut twisted tape and solid twisted tape (Khfagi et al., 2022). In this study, numerical assessment was performed to optimise the mixed convective heat transmission rate and production of entropy in a TECT with an Al_2O_3-Cu/water hybrid-nanofluid as the working fluid. In addition, this paper compares the results generated by mixed convection and those generated by forced convection.

2 Numerical analysis

2.1 Physical model and boundary conditions

In this work, the mixed convection of hybrid nanofluid (Al_2O_3-Cu/water) in a vertical pipe fitted with elliptical-cut twisted tape and uniform wall heat flux has been considered. The following physical models were defined and implemented in Star CCM+ software. The steady state, three-dimensional, segregated flow temperature; the Reynolds averaged Navier-Strokes, and the force of gravity acting in the direction of flow. The realizable k-ε turbulence model was applied to predict the flow of turbulent fluid. The buoyancy force influences the thermophysical properties equation of hybrid nanofluids, which is considered Newtonian. Boussinesq's hypothesis states that the fluid's physical parameters remain constant, except for body force density, which changes linearly with temperature. Viscous dissipation was also included in this work.

The boundary conditions employed in this investigation were as follows.

(1) Figure 1 and Table 1 display the model's geometry, which consists of a tube with elliptical-cut twisted tape inserts.

(2) For the thermal boundary condition, a constant heat flux of 4000 Wm^{-2} was applied to the tube wall, while the elliptical-cut twisted tape is assumed to be adiabatic. Moreover, the twisted tape and the wall of the tube were under a no-slip condition (Khfagi et al., 2022).
(3) Simulations were performed for Reynolds numbers 7000, 9000, 11000, 13000, and 15000 (Saysroy & Eiamsa-ard, 2017)
(4) Al_2O_3-Cu/water hybrid nanofluids were used at concentration ranging from 1% to 4%.

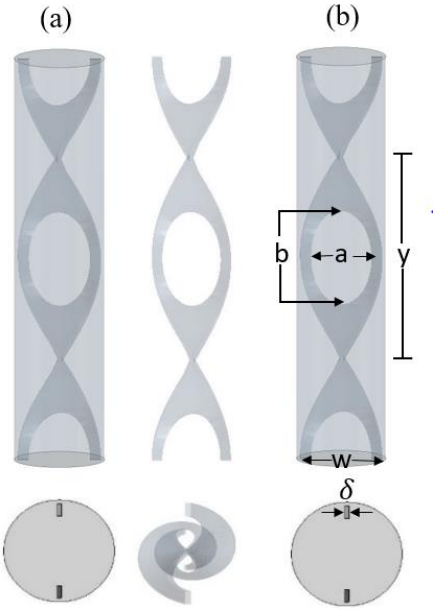

Figure 1. Physical model of (a) TECT, and (b) relevant dimensions in the condition studied.

Table 1. Geometrical parameters of the studied parabolic trough receiver (Ahmadi, Khanmohammadi, Khanmohammadi, Bahiraei, & Bach, 2020; Khfagi et al., 2022)

Feature	Value	Feature	Value
a	0.0133 m	*y*	0.057 m
b	0.00665 m	*δ*	0.0008 m
D	0.0195 m	*a/w*	0.7
L	1 m	*b/a*	2
w	0.019 m		

2.2 Thermal and physical characteristics of hybrid nanofluids

As indicated in Table 2, the thermo-physical properties of pure water, Al_2O_3, and Cu are identified using the methodology in Ref. (Ghasemi & Aminossadati, 2010). Assuming a homogenised mixture, the hybrid nanofluid's thermophysical characteristics are represented by (Alshare, Al-Kouz, & Khan, 2020; Anuar, Bachok, & Pop, 2020; Ghadikolaei, Yassari, Sadeghi, Hosseinzadeh, & Ganji, 2017; Takabi & Salehi, 2014):

Density $(\rho)_{hnf}$:

$$\rho_{hnf} = (1 - \emptyset_{hnf})\rho_f + \emptyset_A\rho_A + \emptyset_C\rho_C \quad (1)$$

Where *A* and *C* denote aluminium oxide (Al_2O_3) and copper (Cu), respectively.

$\emptyset_{hnf}$ is the volume concentration of two distinct nanoparticle forms scattered in hybrid nanofluid and is computed as:

$$\emptyset_{hnf} + \emptyset_A + \emptyset_C \quad (2)$$

Specific heat $(C_p)_{hnf}$:

$$(\rho C_p)_{hnf} = (1-\emptyset_{hnf})(\rho C_p)_f + \emptyset_A(\rho C_p)_A + \emptyset_C(\rho C_p)_C \quad (3)$$

Buoyancy $(\beta)_{hnf}$:

The coefficient of thermal expansion of hybrid nanofluids may be computed using the following formula, which has been cited in several publications (Mehryan, Kashkooli, Ghalambaz, & Chamkha, 2017; Nimmagadda & Venkatasubbaiah, 2015; Takabi & Salehi, 2014):

$$(\rho\beta)_{hnf} = \left(1-\emptyset_{hnf}\right)(\rho\beta)_f + \emptyset_A(\rho\beta)_A + \emptyset_C(\rho\beta)_C \quad (4)$$

Dynamic viscosity $(\mu)_{hnf}$:

$$\mu_{hnf} = \frac{\mu_f}{(1-\emptyset_A)^{2.5}(1-\emptyset_C)^{2.5}} \quad (5)$$

Thermal conductivity $(k_c)_{hnf}$:

$$\frac{(k_c)_{hnf}}{(k_c)_f} = \left(\frac{(\emptyset_A\,(k_c)_A + \emptyset_C\,(k_c)_C)}{\emptyset_{hnf}} + 2(k_c)_f + 2(\emptyset_A(k_c)_A + \emptyset_C(k_c)_C) - 2\emptyset(k_c)_f\right) / \left(\frac{(\emptyset_A\,(k_c)_A + \emptyset_C\,(k_c)_C)}{\emptyset_{hnf}} + 2k_f - (\emptyset_A(k_c)_A + \emptyset_C(k_c)_C) + \emptyset(k_c)_f\right) \quad (6)$$

Here, $\emptyset_A$ and $\emptyset_C$ denote the volume fraction of solid aluminium oxide particles and solid copper nanoparticles, respectively, *f* is base fluid, and *hnf* is hybrid nanofluid.

$(k_c)_{hnf}$, $(k_c)_f$, $(k_c)_A$, and $(k_c)_c$ are the thermal conductivity of hybrid nanofluid, base fluid, aluminium oxide, and copper, respectively.

Table 2. The thermophysical characteristics of the fluid and nanoparticles (Mehryan et al., 2017)

Substances	$\boldsymbol{\rho}$ / Kg m^{-3}	C_p /J Kg^{-1} K^{-1}	$\boldsymbol{k_c}$/ Wm^{-1} K^{-1}	$\boldsymbol{\beta \times 10^{-5}/\ K^{-1}}$
Water	997.1	4179	0.613	21
Al_2O_3	3970	765	40	0.85
Cu	8933	385	400	1.67

2.3 Governing equations

The governing equations for the problem are based on the balance of mass, momentum, and thermal energy. There is an assumption that the working fluid (hybrid-nanofluid) is incompressible and stable. In light of the aforementioned assumptions, continuity, momentum, and energy in three-dimensional equations may be expressed as shown below (Versteeg & Malalasekera, 2007). The fluid's characteristics are formulated as constants, except for the density. It is determined by the temperature difference between the local point and the reference point and can be calculated as (Yan, 1994).

$$(\rho)_{hnf} = \rho_0\left[1-\beta_{hnf}(T-T_0)\right] \quad (7)$$

A hybrid nanofluid's governing equations may be written in terms of these assumptions:

The continuity equation:

$$\frac{\partial}{\partial x_i}(u_i) = 0 \quad (8)$$

Transport of momentum:

$$\frac{\partial}{\partial x_j}\left(u_i u_j\right) = \frac{1}{\rho_{hnf}}\left[-\frac{\partial P}{\partial x_i} + (\mu_{hnf})_{eff}\left(\frac{\partial^2 u_i}{\partial {x_j}^2}\right)\right] - \rho_{hnf}\beta_{hnf}(T-T_0)g \quad (9)$$

The buoyancy factor in equation (9) is approximated using the Boussinesq model (Fluent, 2006) as

$$(\rho_{hnf} - (\rho_{hnf})_0)g \approx -\rho_{hnf}\beta_{hnf}(T - T_0)g \quad (10)$$

Transport of energy:

$$\frac{\partial(u_i T)}{\partial x_i} = \frac{\partial}{\partial x_i}\left[\left(\frac{(k_c)_{hnf}}{(\rho c_p)_{hnf}} + \frac{(\mu_{hnf})_t}{(\rho)_{hnf} Pr_t}\right)\frac{\partial T}{\partial x_i}\right] \quad (11)$$

Where $u, \rho, k_c, \mu,$ and T indicate velocity, density, thermal conductivity of fluid, dynamic viscosity, and time-averaged temperature, respectively. Here $i = 1,2,3, u_i = (v_x, v_y, v_z)$ are vectors of velocity in the x, y, and z directions, respectively.

Equations for transport in the realizable *k*-ε model:

The realizable *k*-ε model (Shih, 1993) is a relatively modern evolution. The realizable *k*-ε model is more capable in predicting flow velocities in complex flow geometries such as twisted tape inserts.

The following expression describes the realizable *k*-ε turbulence model.
Turbulence kinetic energy equation (k):

$$\frac{\partial(\rho_{hnf}k)}{\partial t} + \frac{\partial(\rho_{hnf}ku_i)}{\partial x_i} = \frac{\partial}{\partial x_j}\left[\left((\mu_{hnf}) + \frac{(\mu_{hnf})_t}{\sigma_k}\right)\frac{\partial k}{\partial x_j}\right] + G_b + G_k - \rho\varepsilon - Y_M + S_k \quad (12)$$

Equation of turbulence dissipation rate (ε)

$$\frac{\partial(\rho_{hnf}\varepsilon)}{\partial t} + \frac{\partial(\rho_{hnf}\varepsilon u_i)}{\partial x_i} = \frac{\partial}{\partial x_j}\left[\left((\mu_{hnf}) + \frac{(\mu_{hnf})_t}{\sigma_\varepsilon}\right)\frac{\partial \varepsilon}{\partial x_j}\right] + \rho_{hnf}C_1 S_\varepsilon - \rho C_2 \frac{\varepsilon^2}{k + \sqrt{(\mu/\rho)\varepsilon}} + C_{1\varepsilon}\frac{\varepsilon}{k}C_{3\varepsilon}P_b + S_\varepsilon \quad (13)$$

where: $C_1 = max\left[0.43, \frac{\eta}{\eta+5}\right]$, $\eta = S\frac{k}{\varepsilon}$,

S is expressed by the velocity strain rate tensor $S \equiv \sqrt{2S_{ij}S_{ij}}$,

Here G_k represents the kinetic energy created by the turbulence, and was developed in the same way as the other the *k*-ε models as:

$$G_k = (\mu_{hnf})_t S^2 \quad (14)$$

The eddy viscosity is given by

$$(\mu_{hnf})_t = \rho C_{\mu_{hnf}} \frac{k^2}{\varepsilon} \quad (15)$$

The effective viscosity could be determined as follows: $(\mu_{hnf})_{eff} = \mu_{hnf} + (\mu_{hnf})_t$.

Y_M is compressibility modification. $Y_M = C_{\mu_{hnf}} k\varepsilon\, C_2$

All other empirical constants are described by (Versteeg & Malalasekera, 2007):

$C_{1\varepsilon} = 1.44, C_2 = 1.9, \sigma_\varepsilon = 1.2, \sigma_k = 1.0.$

In this work, the buoyant shear layers $C_{3\varepsilon} = 1$, due to gravity aligning with the main flow direction.

2.4 Evaluation of parameters

The simulation results and the flow and heat transmission in the TECT are described with showing the dimensionless parameters and certain variables.

The Reynolds number value (Re):

$$Re = \frac{\rho\, u\, D}{\mu} \tag{16}$$

The Grashoff number (Gr) is determined to be (Karwe & Deo, 2003)

$$Gr = \left(\frac{g\beta(T-T_0)L^3\rho_{hnf}^2}{\mu_{hnf}^2}\right) \tag{17}$$

The Richardson number (Ri) is calculated to be (Patil & Vijay Babu, 2012)

$$Ri = \frac{Gr}{Re^2} \tag{18}$$

The Nusselt number (Nu) is expressed as (Bergman, Bergman, Incropera, Dewitt, & Lavine, 2011):

$$Nu = \frac{1}{L}\int_0^L Nu(x)dx \tag{19}$$

The friction factor (f) for fully developed flow is computed by determining the pressure drop (Δp) for TECT as follows (Oni & Paul, 2016).

$$f = \frac{2\,\Delta p\, D}{\rho\, Lu^2} \tag{20}$$

The ratio of convection heat transport and friction factor is employed in this study to calculate the thermal efficiency factor for TECT (Khfagi et al., 2022).

The factor of thermal performance is described as following:

$$\eta = \frac{\left({}^{Nu}/_{Nu_p}\right)}{\left({}^{f}/_{f_p}\right)^{1/3}} \tag{21}$$

2.5 Entropy generation

For each condition, the local volumetric entropy production rate was measured, with thermal and frictional effects being the sole contributors:

$$S_{g,t} = S_{HT} + S_{FF} \tag{22}$$

Typically, the production of volumetric entropy in a system is represented as shown below (Zimparov, 2001)

$$S_{HT} = \frac{k_c}{T^2}\left(\frac{\partial T}{\partial x_i}\right)^2 \tag{23}$$

$$S_{FF} = \frac{\mu_{hnf}}{T}\left\{2\left[\left(\frac{\partial u_i}{\partial x_i}\right)^2\right] + \left(\frac{\partial u_i}{\partial x_j} + \frac{\partial u_j}{\partial x_i}\right)^2\right\} \tag{24}$$

A sum of volumetric entropy production components is integrated over the volume of the pipe, the total entropy production ($S_{g,t}$) is computed.

$$S_{g,t} = \{\int S_{HT} + \int S_{FF}\}\,\partial V \tag{25}$$

The Bejan number is usually employed to illustrate how much each irreversibility contributes to the rate at which the generation of total entropy occurs. A definition of the Bejan number is (Sheikholeslami, Jafaryar, & Li, 2018)

$$Be = \frac{S_{HT}}{S_{g,t}} \tag{26}$$

2.6 Numerical techniques

Commercial CFD software, Star-CCM+, was used to perform mathematical simulations of turbulent flow in a TECT. The convective and diffusive terms were handled using upwind approaches of second order, while the pressure–velocity coupling was handled using the SIMPLE (Semi-Implicit Pressure Linked Equations) technique suggested by (Patankar & Spalding, 1983). The governing equations were thoroughly evaluated by Versteeg and Malalasekera (Versteeg & Malalasekera, 2007). The realizable k– ε model is being employed in this study as the turbulence model. The solution was obtained with a Grashorf number of 4.028×10^{8}. The thermophysical properties and the coefficient of thermal expansion of hybrid-nanofluid at different volume concentrations are calculated by the equation in section 2.2. The thermal efficiency factor was estimated using Equation (21) to assess the performance improvement. At various points, mass conservation, energy conservation, and temperature were measured to determine the convergence of solutions. The momentum and energy equations were defined utilizing the second order upwind technique. Equations (23) to (26) were also solved in MATLAB.

3 Grid independence test and model validation

Grid independence study on temperature for different mesh sizes was carried out to discover a suitable grid with high accuracy in order to assure the correctness of the computations. As part of this analysis, the grid independence test was conducted on the realizable k-ε turbulence model for a Reynolds number of 11000 in a vertical TECT to choose an appropriate grid for resolving the flow inside the domain. Five distinct grids containing the numbers 2615663, 2892319, 2990608, 3359202 and 3413798 were used. To do this, the temperature at the domain's exit was calculated from the cross-section as displayed in Figure 2 (a). According to this figure, there are some discrepancies in the temperature readings of the grids. The grids with 2615663, 2892319, 2990608, and 3413798 cells differ by 0.2%, 0.1%, 0.5%, and 0.09%, respectively, compared with the grids with 3359202 cells. These grids were selected in this work.

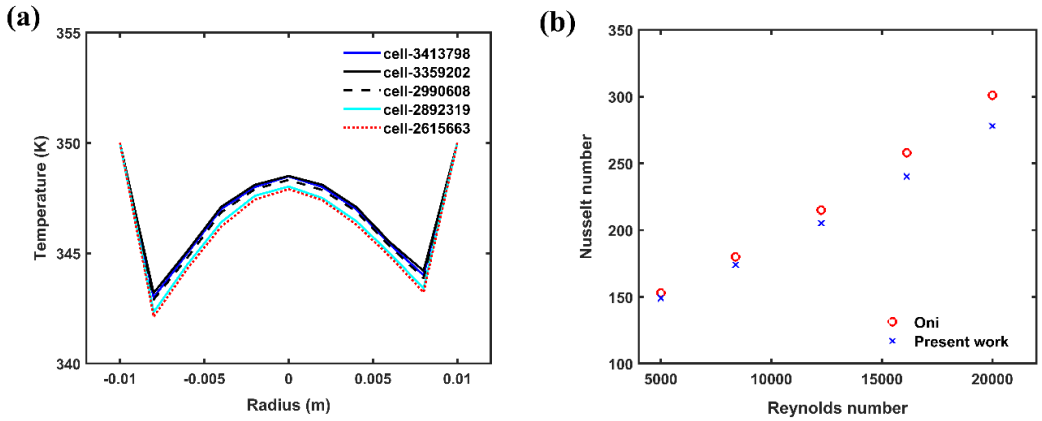

Figure 2. (a) Grid independence tests (b) Nusselt number against Reynolds number, Oni and Paul (Oni & Paul, 2015).

In our earlier work (Khfagi et al., 2022), the Nusselt number, the factor of thermal efficiency, and friction factor determined for forced convection using the realizable k-ε model of TECT were compared with Ahmadi's (Ahmadi et al., 2020) work for varied nanoparticle mass concentrations and a Reynolds number of 7000. In Figure 2 a pipe made with a twisted tape cut in the shape of an alternate-axis triangle (TATCT) from Oni and Paul (Oni & Paul, 2015) was used to validate our tube model (TECT) for mixed convection at 15˚and turbulent flow at $5000 \leq Re \leq 20000$. The results were found with a Grashorf number and Prandtl number of 3.37×10^{5} and 5.83 respectively. The mixed convection Nusselt numbers for TECT and TATCT were compared, and the findings are displayed in Figure 2 (b). Apparently, the Nusselt numbers of the present TECT deviated from those of TATCT by ± 8.3%. Comparing the results demonstrates excellent agreement under turbulent flow conditions, confirming the reliability of the present numerical method.

4 Results and discussion

4.1 Temperature fields

The temperature fields of an Al_2O_3/Cu-water hybrid-nanofluid (Ø =2%) flows are displayed in Figure 3. The findings for the distribution of temperature in the tubes obtained for turbulent flows are shown in Figure 3, frames (a - f), (a) forced convection at (Re = 7000), and (b-f) convection of mixed at Reynolds numbers of (b) 7000, (c) 9000, (d) 11000, (e) 13000, and (f) 15000. At Reynolds numbers of 7000 (Figure 3, frames a and b), the buoyancy influence caused a density differential in the fluid Al_2O_3-Cu/water hybrid nanofluid, leading to a higher temperature in the mixed convection pipe than in the forced convection pipe. In mixed convection, the tube temperature slightly rose as the Reynolds number improved. The temperature slowly develops along the pipe noticeably (Figure 3, frames b - f). This is in agreement with Oni and Paul (Oni & Paul, 2015).

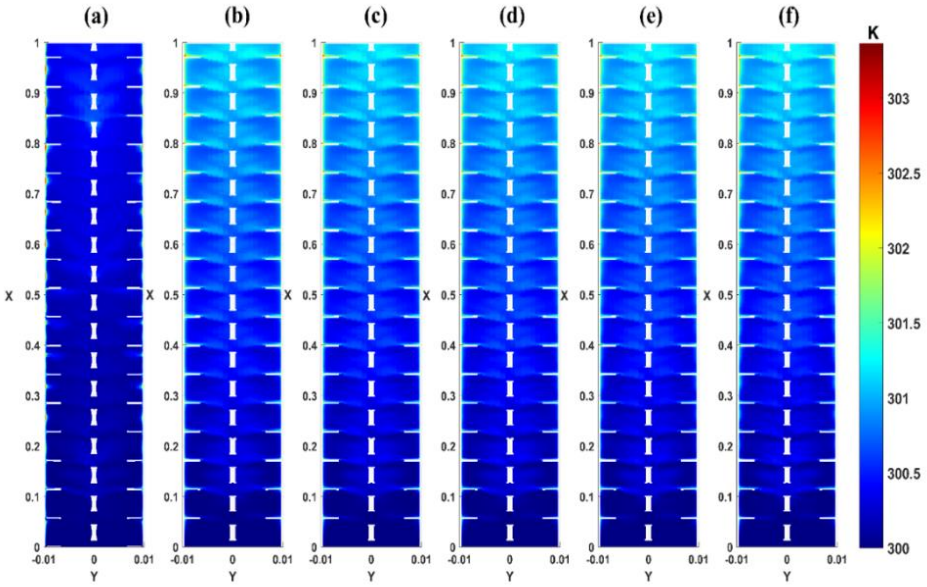

Figure 3. Temperature contour (a) forced convection Re =7000 (b) mixed convection Re=7000 (c) mixed convection Re=9000 (d) mixed convection Re=11000 (e) mixed convection Re=13000 and (f) mixed convection Re=15000.

4.2 Turbulence kinetic energy

At Re = 7000 and Ø = 2 %, Figure 4 (Frames a and b) presents the turbulence kinetic energy differences in the forced convection and the mixed convection, respectively. The turbulence kinetic energy gradually increases until it reaches the end of the tube. The maximum turbulence kinetic energy of TECT in forced convection (frame a) was around 65% lower than in TECT with mixed convection (frame b). In Figure 4 (frames a - f), the kinetic energy of turbulence around the tape cuts is significantly larger than the turbulence kinetic energy in the surrounding area. In Oni and Paul's (Oni & Paul, 2015) viewpoint, this is due to the disruptions the cuts cause to the flow. It is clear that when Reynolds numbers approach (b) 7000, (c) 9000, (d) 11,000, (e) 13,000, and (f) 15000, the turbulence kinetic energy improves significantly. There is an increase in the kinetic energy of turbulence when the Reynolds number rises because of the increasing velocity (Oni & Paul, 2015).

4.3 Heat transfer by mixed convection

Table 3 displays the correlation between Reynolds and Richardson numbers. As seen in Table 3, the Richardson Number drops as the Reynolds Number rises because of higher forced convection. The buoyancy effects are generally disregarded at the high Reynolds numbers of the imposed forced flow (Patil & Vijay Babu, 2012). Table 3 also reveals that heat transfer rates are greater for $Ri \geq 1$ than for pure forced convection, showing that free convection impacts dominate over forced convection impacts, similar to that of Ref. (Patil & Vijay Babu, 2012).

Table 3. Reynolds number vs Richardson number in TECT for Al_2O_3-Cu/water

Re	7000	9000	11000	13000	15000
Ri	8.22	4.97	3.33	2.38	1.79

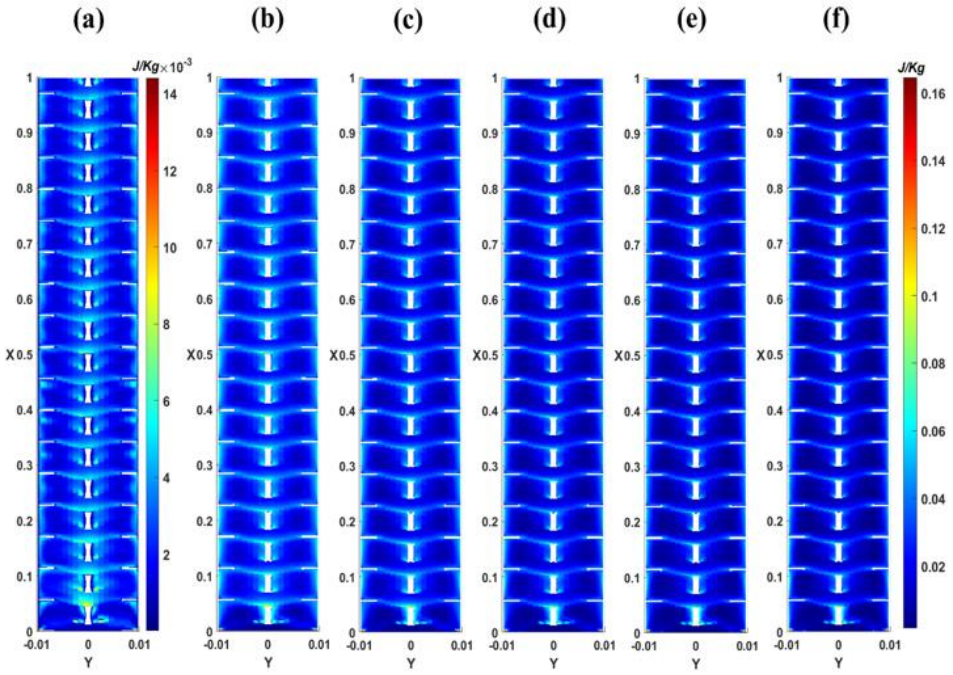

Figure 4. Turbulence kinetic energy contour (a) forced convection Re =7000 (b) mixed convection Re=7000 (c) mixed convection Re=9000 (d) mixed convection Re=11000 (e) mixed convection Re=13000 and (f) mixed convection Re=15000.

4.4 Outlet temperature and velocity

Figure 5 (a) depicts the impact of nanoparticle concentrations at varying Reynolds numbers on the outlet temperature for turbulent Al_2O_3-Cu/water hybrid nanofluids. In this case, raising the Reynolds number resulted in a drop in the output temperature. When the concentration of nanoparticles rose, however, the normalised temperature dropped slightly. As a result, while raising $\emptyset_{hnf}$ from 1 to 4%, the outlet temperature is reduced by around 9.4%. Therefore, if the mass flow rate stays the same and the particle concentration goes up, it results in a degradation of the secondary motion due to buoyancy forces. This is because the addition of nanoparticles leads to a considerable rise in dynamic viscosity compared to pure water, particularly at high nanoparticle concentrations. These findings demonstrate that effective thermal conductivity alone is insufficient to fully define the heat transfer behaviour of nanoparticles. Various physical variables (density, heat capacity, thermal expansion coefficient) can influence nanoparticle heat transmission characteristics in forced convection (Mansour, Galanis, & Nguyen, 2007) and free convection (Polidori, Fohanno, & Nguyen, 2007). Figure 5 (b) demonstrates the impact of nanoparticle concentrations on the outflow velocity for turbulent hybrid nanofluids. The figure demonstrates that the average outlet velocity raises as the Reynolds number and nanoparticles rise due to thermophysical properties. Therefore, when $\emptyset_{hnf}$ goes from 1 to 4%, the average outlet velocity goes up by about 10.9%.

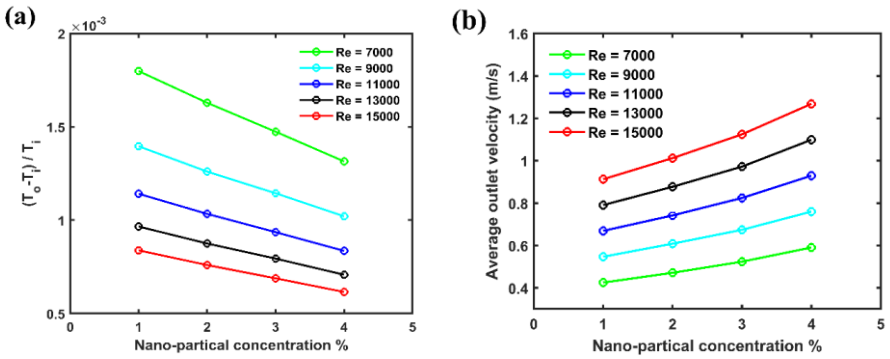

Figure 5. (a) Average output temperature vs various nanoparticle concentrations with various Reynolds numbers (b) Average output velocity vs various nanoparticle concentrations with various Reynolds numbers.

4.5 Nusselt Number

In this analysis, heat transmission was evaluated using the Nusselt number. Figure 6 (a-d) exhibits the comparison of Nusselt numbers for mixed and forced convection at different nanoparticle concentrations. Mixed convection had a higher Nusselt number than forced convection, at 4.6% higher. Mixed convection improves heat transmission by using both natural and forced convection simultaneously, resulting in three distinct processes. These processes consist of the external force provided by forced convection, while natural convection generates buoyancy forces with parallel and normal components. Forced convection lowered thermal resistance and boosted heat transfer because of the external force. When the force of buoyancy was applied in the same direction as the tube's primary flow, thermal resistance decreased, and heat transmission increased. The buoyancy force's natural component disrupted the boundary layer, resulting in increased heat transmission (Maughan & Incropera, 1987; Oni & Paul, 2015). Figure 7 illustrates the impact of the concentration of nanoparticles in TECT on heat transmission for hybrid Al_2O_3–Cu/water nanofluid flow at varying Reynolds numbers. Heat transfer is improved, as expected, with both an elevated Reynolds number as well as a nanoparticle concentration. According to (Khfagi et al., 2022; Vajjha & Das, 2008), the reason is that, as the number of nanoparticles rises, the thermal conductivity increases, so the rate of heat transport increases.

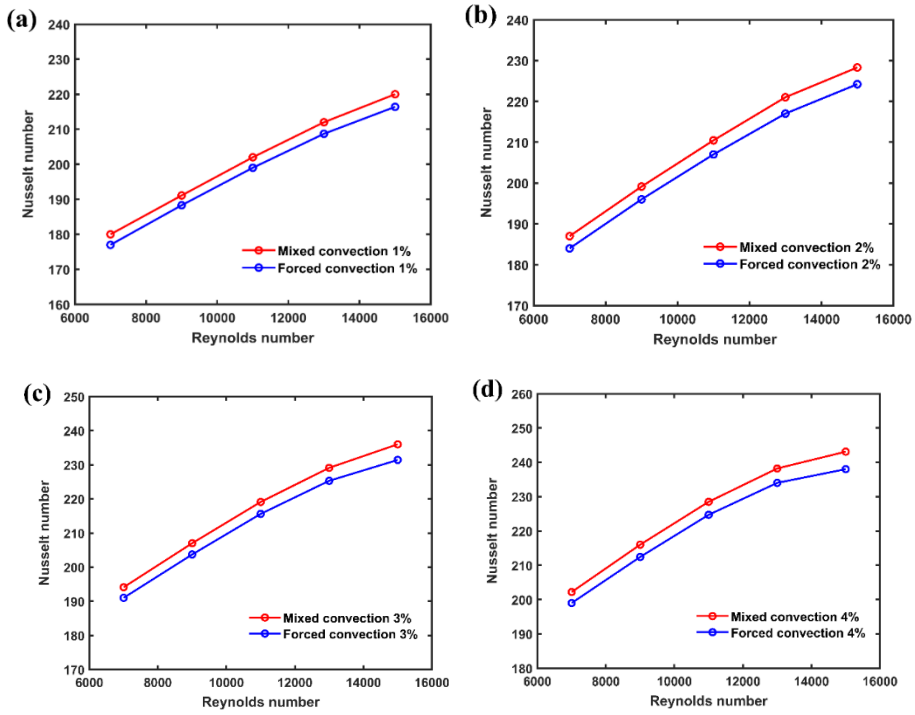

Figure 6. Effect of Nusselt number for various Reynolds numbers with various concentration of Al_2O_3-Cu/water (a) 1%, (b) 2 %, (c) 3 %, and (d) 4%.

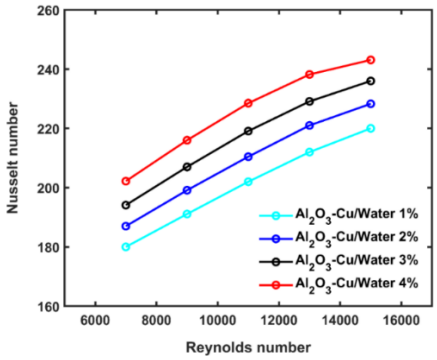

Figure 7. Variation of Nusselt number of Al_2O_3-Cu/water vs Reynolds number at various concentrations of nanoparticles

4.6 Friction Factor

Figure 8 (a) demonstrates the influence of the friction factor on the Reynolds number in both forced and mixed convection flows at (∅ =2%). As predicted, forced convection has a lower coefficient of friction than the mixed convection. The force of buoyancy caused by free convection operating on the flow, as well as the forces caused by forced convection operating on the flow, are responsible for this (Oni & Paul, 2015). The friction factor was up to 13.6% higher in tubes with elliptical tape for mixed convection than in tubes with forced convection. Figure 8 describes the influence of different nanoparticle concentrations on the friction factor for (b) mixed and forced convection at Re = 11,000, and (c) with different Reynolds numbers. As illustrated, friction factor values are found to be consistent across all tested nanoparticle concentrations. This is owing to the Reynolds number and surface coarseness having the greatest influence on the friction factor (Ahmadi et al., 2020; Khfagi et al., 2022).

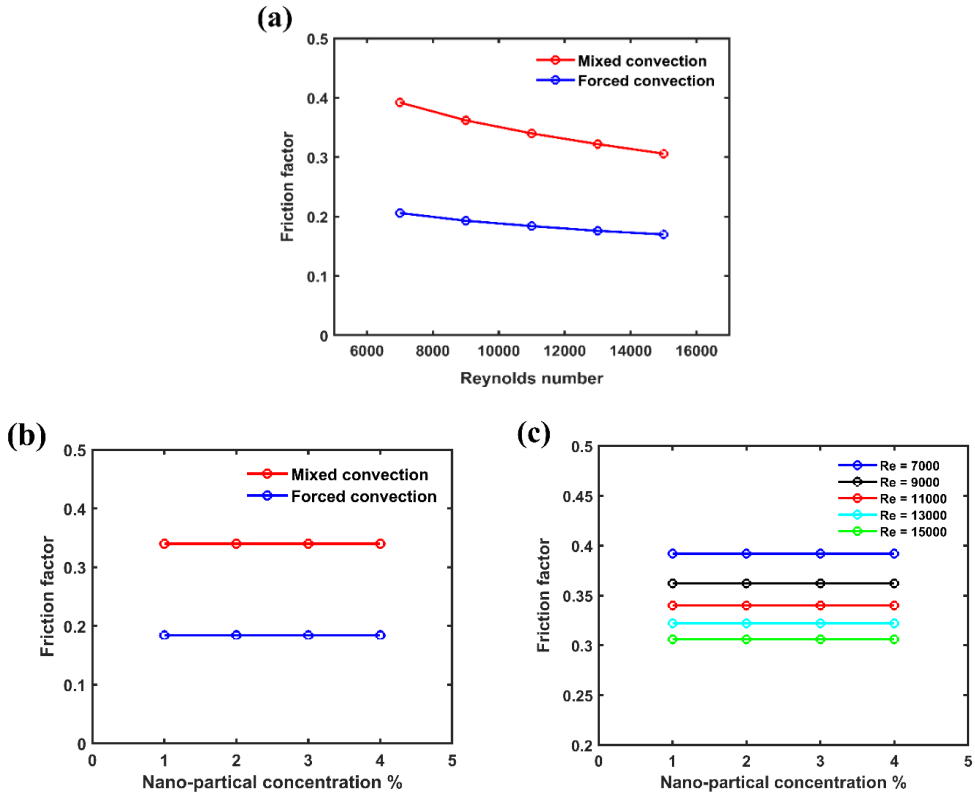

Figure 8. Friction factor variation (a) in relation to Reynolds number at (∅ =2 %), (b) with different nanoparticle concentrations of mixed and forced convection at Re = 11,000, and (c) with different nanoparticle concentrations at different Reynolds numbers.

4.7 Thermal performance factor (TPF)

Figure 9 (a-d) illustrates the correlation between the variation of the thermal performance factor and the Reynolds number of mixed convection and forced convection at different nanoparticle concentrations. The findings demonstrate an improvement in the rate of heat transmission for mixed convection. The thermal performance factor for mixed convection exceeded that for forced convection. Even though the use of mixed convection results in an increase in friction factor, as stated in the preceding section, thermal performance is improved due to a moderate rise in heat transmission rate (Oni & Paul, 2014). Quantitatively, mixed convection had a thermal performance factor that was up to 5.5% higher than forced convection.

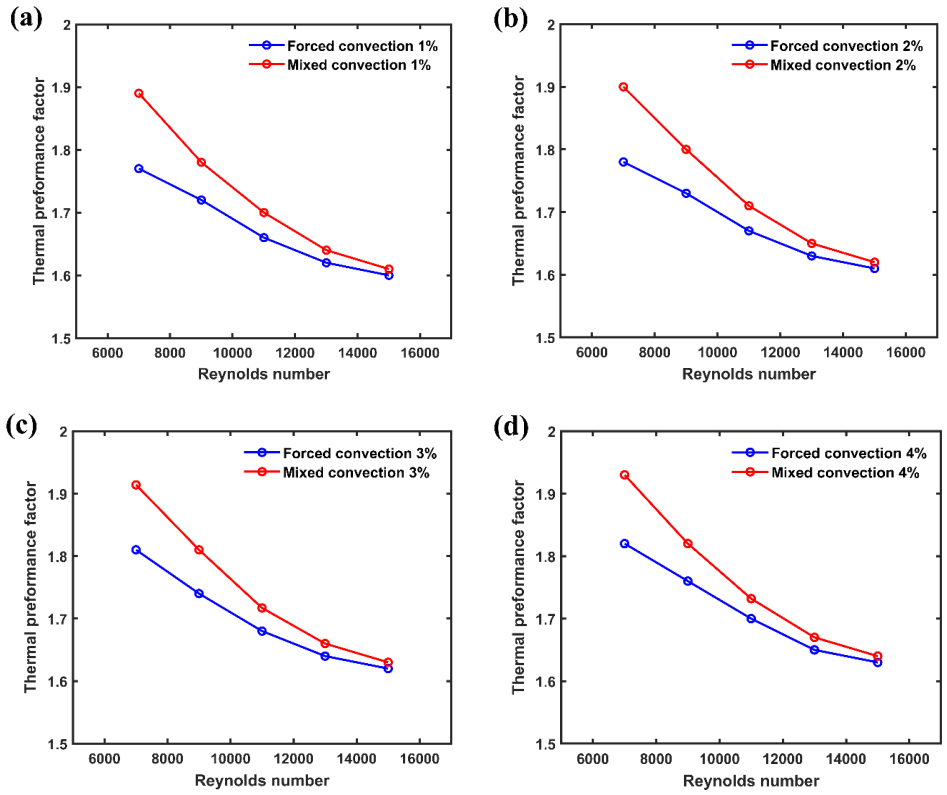

Figure 9. The effect of the thermal performance factor on the Reynolds Number for Al_2O_3-Cu/water (a) ∅ =1%, (b) ∅ =2 %, (c) ∅ =3 %, and (d) ∅ =4%.

4.8 Entropy Generation analysis

This section includes an examination of the generation of entropy during mixed convection for TECT of an Al_2O_3-Cu/water hybrid nanofluid at ∅ = 2% for Reynolds numbers from 7000 to 15000. Furthermore, the production total entropy and Bejan number of an Al_2O_3-Cu/water hybrid nanofluid are examined at ∅ from 1% to 4%. The irreversibilities (entropy) are generated due to irreversible fluid friction and heat transmission (Zimparov, 2001). Entropy is created in thermal systems via heat transmission owing to a temperature differential and the irreversible dissipation of kinetic energy from fluid friction (Zimparov, 2001). A major purpose of this study is to evaluate the impact of mixed convection in the TECT within the entropy production principles, considering solely the effects of friction of fluid and transfer of heat.

4.8.1 The local entropy generation

Figures 10-12 depict the evolution of local entropy generation and local Bejan numbers. Figure 10 describes the local distribution of thermal entropy production for several Reynolds numbers (a) 7000, (b) 9000, (c) 11000, (d) 13000, and (e) 15000. The findings reveal that the highest thermal entropy production in TECT arises near the walls of the channel and the surface of the twisted tape, where the temperature differential is greatest. This is because the elliptical-cut twisted tape creates a strong swirl flow in the duct, thus enhancing entropy production due to heat transmission (Khfagi et al., 2022). Furthermore, the entropy generation of thermal has negligible values across wider cross sections at

greater Reynolds numbers because the layer of thermal boundary expands more slowly at higher Reynolds numbers. This is consistent with the findings of Refs (Bahiraei, Jamshidmofid, & Heshmatian, 2017; Esfahani, Akbarzadeh, Rashidi, Rosen, & Ellahi, 2017). For turbulent flows, the thermal part of the rate of entropy production is no longer dependent only on conductivity, it depends on viscosity too (Singh, Anoop, Sundararajan, & Das, 2010). In addition, as the buoyancy effect increases, the density of the fluid varies as well as when the Reynolds number grows. Moreover, the thermal conductivity in the system rises, while it reduces towards pipe walls and twisted tape surfaces (Bahiraei et al., 2017). At different Reynolds numbers, the different thermal conductivities and temperature distributions affect both the quality of the temperature gradient changes and the way the layer of thermal boundary develops. Because the thermal conductivity near the wall and twisted tape is reduced as Reynolds numbers rise, the gradient of temperature in these places increases more than normal, which has an influence on the rate of thermal entropy production (Bahiraei et al., 2017). Figure 11 depicts the local distribution of frictional entropy production for several Reynolds numbers (a) 7000, (b) 9000, (c) 11000, (d) 13000, and (e) 15000. As can be observed, the Reynolds number enhances frictional entropy formation. Reynolds number enhances the velocity gradient and frictional entropy production. As demonstrated in Figure 11, the entropy production due to fluid friction around the elliptical-cut twisted tape rotational axis increases significantly. This rise is caused the use of twisted tape in this area, which makes flow velocity gradients bigger (Khfagi et al., 2022). Figure 12**Figure *12*** illustrates the local distribution of the Bejan number for Reynolds numbers (a) 7000, (b) 9000, (c) 11000, (d) 13000, and (e) 15000. As a consequence, the local Bejan number's contour is almost symmetric. In Figure 12 (frames a-c), the Bejan number range is between 0.8 and 1.0, showing that irreversible heat transfer occurs throughout the pipe. However, the range of Bejan numbers in (frames d-e) is less than 0.8, indicating that fluid friction irreversibilities are dominant throughout the pipe (Zadeh, Mehryan, Islam, & Ghalambaz, 2020).

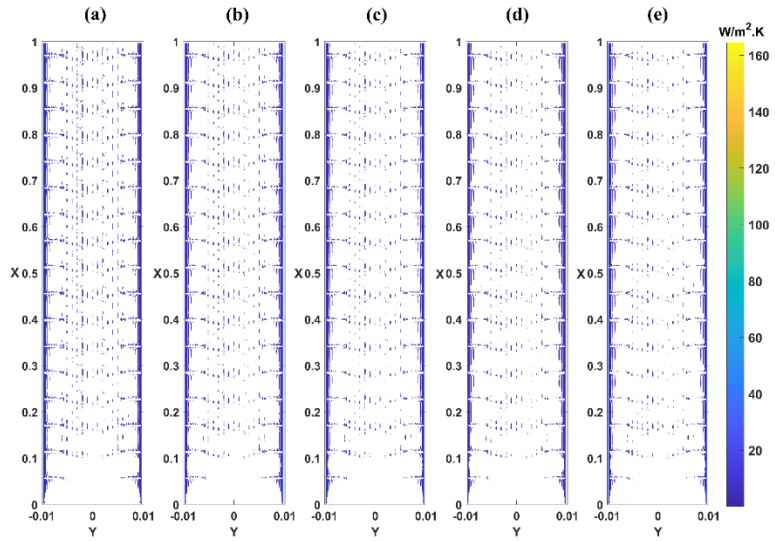

Figure 10. Spatial distribution of thermal entropy generation for (a) Re= 7000 (b) Re= 9000 (c) Re= 11000 (d) Re= 13000 and (e) Re= 15000.

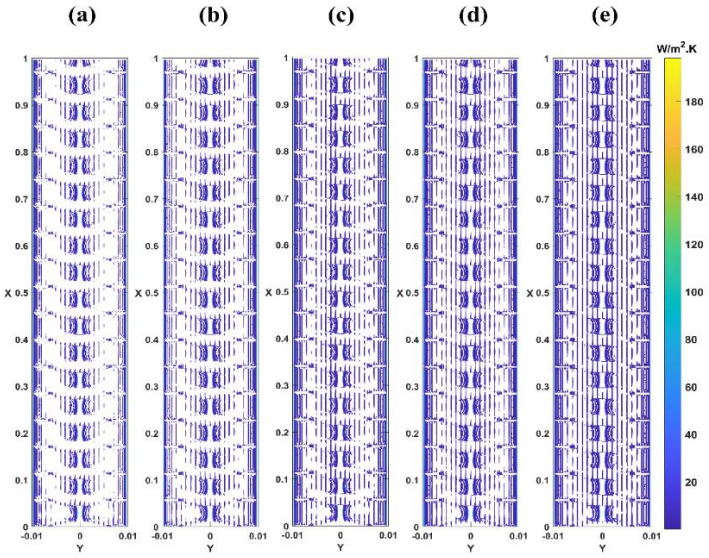

Figure 11. Spatial distribution of frictional entropy generation for (a) Re= 7000 (b) Re= 9000 (c) Re= 11000 (d) Re= 13000 and (e) Re= 15000.

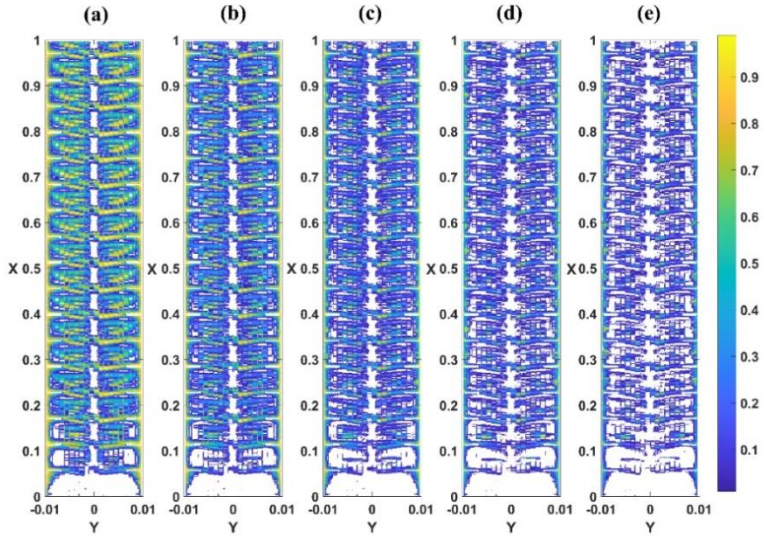

Figure 12. Bejan number for (a) Re= 7000 (b) Re= 9000 (c) Re= 11000 (d) Re= 13000 and (e) Re= 15000.

4.8.2 Total entropy generation and Bejan number

As previously stated, entropy generation consists of two components: irreversibility of fluid friction and transfer of heat between finite temperatures. Figure 13 (a and b) demonstrate the fluctuation of these components and their respective contribution to the generation of total entropy with an improving Reynolds number. Figure 13 (a) illustrates a comparison of thermal entropy production for mixed and forced convection. As the Reynolds number rises, it can be observed that the rate of thermal entropy creation reduces. It should be mentioned that heat transmission is enhanced as the Reynolds number rises. Moreover, the mixed convection heat transmission rate was greater than forced convection (section 4.5). Consequently, thermal entropy production is minimized as the thermal gradients in the flow field decrease (Mwesigye, Bello-Ochende, & Meyer, 2014). Further, this analysis shows that the generation of thermal entropy is concentrated in the region close to the channel wall and twisted tape due to the greatest temperature gradient. Note also that a small amount of thermal entropy is generated between the tube's wall and the twisted tape (Figure 10). Thus, the temperature gradient in this area is reduced due to the formation of a secondary flow region. Quantitatively, mixed convection had a lower thermal entropy generation rate than forced convection, at 40% lower. Figure 13 (b) provides a study of frictional entropy production for mixed and forced convection versus different Reynolds numbers.

As can be understood, in mixed and forced convection, the rate of frictional entropy creation becomes more intense when the Reynolds number rises. The primary cause for such an increase is related to the velocity gradient increment (Khfagi et al., 2022). Figure 14 depicts the variation of total entropy creation for different Reynolds numbers for (a) forced and mixed convection and (b) different Al_2O_3-Cu/water hybrid nanofluid concentrations. Regarding Figure 14 (a), as predicted, mixed convection has a significant impact on the generation of total entropy, such that the greatest decrease in the rate of total entropy formation is 38.45%. It is evident that at lower Reynolds numbers (7000, 9000, and 11000), heat transmission irreversibility is dominat, but fluid friction is dominant at higher Reynolds numbers (13000 and 15000). There is agreement between these results and those in Reference (Mwesigye et al., 2014). Furthermore, total entropy shows a minimum value at about Re = 11000. To show the impact of nanoparticle concentration on the production of total entropy reduction, Figure 14 (b) depicts the total entropy production decrement as a function of the increase in the hybrid nanofluid concentration from 1% to 4%. As depicted in Figure 14 (b), Reynolds number impacts the rate of reduction of total entropy production, with the greatest reduction of 23% and 16.89 occurring under the conditions of Re = 11000 and concentrations of 1% and 2%, respectively. However, the results also demonstrate that the total entropy production rate rises with the rise of Reynolds numbers above 11000 and concentrations of nanoparticles with Reynolds numbers above 7000, which is due to the improvement of the frictional and thermal entropy generation rates (Al-Rashed et al., 2019). At a Reynolds number of 13000, for instance, the total entropy production rate of Al_2O_3-Cu/water hybrid nanofluid concentrations (2%, 3%, and 4%) is increased by 8.8%, 21.1%, and 40.3%, respectively, when the nanoparticle concentration is increased from 1%. Also, raising the Reynolds number from 13000 to 15000 increases the rate of total entropy production of hybrid nanofluids by 18.9 at a nanoparticle concentration of 4%.

Bejan's number illustrates the influence of each irreversibility on the generation of total entropy. The number of Bejan is the ratio of the rate of irreversible thermal entropy formation to the rate of total entropy formation. For Bejan numbers close to one, irreversible heat transfer predominates, while for Bejan numbers close to zero, irreversible fluid friction predominates. For both forced and mixed convection, Bejan numbers vary according to Reynolds numbers (see Figure 15 (a)).

At Re (7000, 9000, and 11000), the Bejan number is found to be near 1 and then drops with rising Reynolds numbers. In mixed convection, the Bejan number is about 0.54 at a Reynolds number of 11,000. According to Varol el at (Varol, Oztop, & Koca, 2008), when Be = 0.5, the rates of frictional and thermal entropy production are equal. At high Reynolds numbers (13000 and 15000), the entropy creation is due to fluid friction irreversibility, leading to a value Bejan number close to zero since the buoyancy-induced flow velocity is high.

Finally, for Reynolds numbers between 7000 and 15000, Figure 15 (b) indicates the impact of nanoparticle shape on the Bejan number at varying concentrations of nanoparticles. Based on the data, it may be deduced that the Bejan number decreases with an increase in nanoparticles and Reynolds number. This means that the ratio of thermal entropy to total entropy decreases and the ratio of frictional entropy increases (Shahsavar, Moradi, & Bahiraei, 2018).

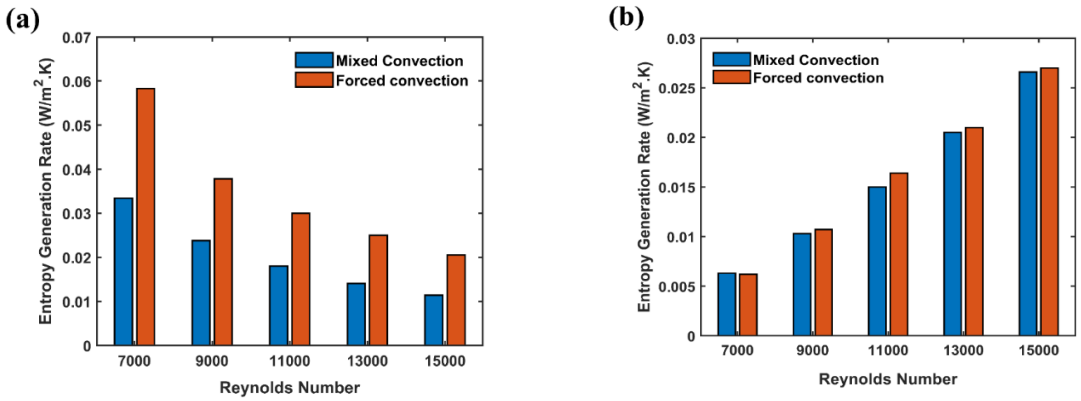

Figure 13. Entropy production due to (a) thermal (b) frictional.

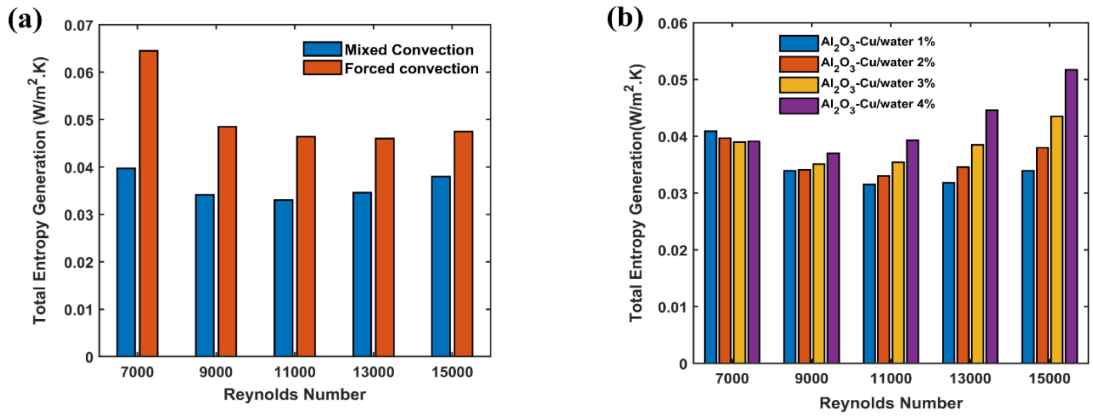

Figure 14. Total entropy production (a) compares between mixed and forced convection at concentration 2% (b) varying concentrations of hybrid nanofluid.

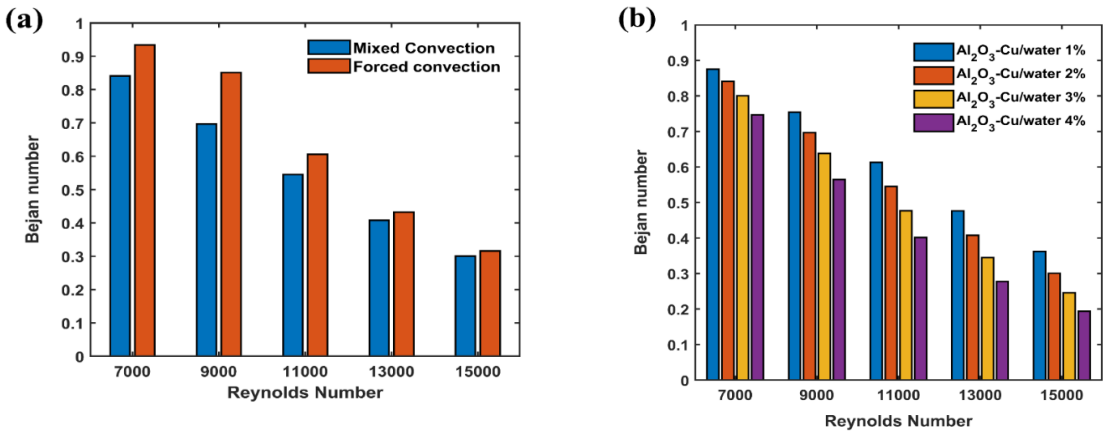

Figure 15. Bejan number against Reynolds number (a) compare between mixed and forced convection at concentration 2% (b) varying concentrations of hybrid nanofluid.

In addition to hybrid nanofluid and geometry of tube, the novel mixed convection also plays in enhancement heat transmission and reduces entropy production. The simulation findings of the proposed mixed convection of Al_2O_3-Cu/water hybrid-nanofluid in (TECT) are illustrated in Table 4. All data used in the comparisons are the best-observed findings in corresponding research. Novel mixed convection achieves better performance in the proposed work.

Table 4. Summary of Research Findings

References	Technique used	Fluids at Re = 7000	Heat transfer enhancement	Improve of thermal performance factor	Minimize total entropy generation
This work	Mixed convection	Al_2O_3-Cu/water	202	1.93	0.039 W/m^2.K
(Khfagi et al., 2022)	Forced convection	Al_2O_3-Cu/water	199	1.82	0.065 W/m^2.K
(Ahmadi et al., 2020)	Forced convection	Nanofluid	199.9	1.7637	Null
(Oni & Paul, 2015)	Mixed convection	Water	180	Null	Null
(Saysroy & Eiamsa-ard, 2017)	Forced convection	Water	112	1.3	Null
(Sheikholeslami et al., 2018)	Forced convection	Nanofluid	Null	Null	0.07 W/m^2.K

5 Conclusions

As a way to gain insight into how nanotechnology might improve heat transfer, this numerical study provided a 3D simulation of turbulent mixed convection flow and analysis of entropy production in TECT of an Al_2O_3-Cu/water hybrid-nanofluid. Calculations were performed using Reynolds numbers ranging from 7000 to 15,000. The governing equations were solved by the finite volume approach using a SIMPLE algorithm. The results obtained are summarised as follows.

- Mixed convection has greater values for the Nusselt number, friction factor, and thermal performance factor than forced convection.
- Also, when the Reynolds number rises, the friction factor and thermal performance factor drop.
- The Nusselt number and the factor of thermal performance for mixed convection were 4.6% and 5.5% higher than for forced convection, respectively.
- Heat transfer is improved with both increased Reynolds numbers and nanoparticle concentrations from 1% to 4%.
- An increase in the Reynolds number leads to a decrease in thermal entropy production and an increase in frictional entropy production.
- Mixed convection has a significant impact on the minimisation of total entropy production.
- Mixed convection reduces total entropy generation by up to 38.45% compared to forced convection.
- Overall, thermal entropy generation appears to be the predominant cause of irreversibility in the problem at Reynolds numbers (7000, 9000, and 11000). Likewise, frictional entropy generation is the predominant mode of irreversibility in the problem at high Reynolds numbers (13000 and 15000). In turn, the minimal value of total entropy occurs at about Re = 11000.

The flow of mixed convection in pipes fitted with twisted tape has not received adequate attention from a second-law analysis perspective. Therefore, further study is needed to fully realise the potential of the field. In addition, research into the Al_2O_3-Cu/water hybrid nanofluid that was studied here is required. This will undoubtedly allow for a comparison of the upcoming results with the existing findings on hybrid-nanofluid. Additionally, an appropriate experiment has to be constructed to further evaluate the simulated outcomes of elliptical-cut twisted tape with the highest performance (TECT).

Acknowledgements

The first author gratefully acknowledges the Ministry of Higher Education and Scientific Research in Libya the funding doctoral studies at Glasgow University.

References

Abdelmeguid, A., & Spalding, D. (1979). Turbulent flow and heat transfer in pipes with buoyancy effects. *Journal of Fluid Mechanics, 94*(2), 383-400.

Aberoumand, S., & Jafarimoghaddam, A. (2016). Mixed convection heat transfer of nanofluids inside curved tubes: An experimental study. *Applied Thermal Engineering, 108*, 967-979.

Ahmadi, K., Khanmohammadi, S., Khanmohammadi, S., Bahiraei, M., & Bach, Q.-V. (2020). Heat transfer assessment of turbulent nanofluid flow in a circular pipe fitted with elliptical-cut twisted tape inserts. *Journal of Thermal Analysis and Calorimetry*, 1-14.

Al-Rashed, A. A., Ranjbarzadeh, R., Aghakhani, S., Soltanimehr, M., Afrand, M., & Nguyen, T. K. (2019). Entropy generation of boehmite alumina nanofluid flow through a minichannel heat exchanger considering nanoparticle shape effect. *Physica A: Statistical Mechanics and its Applications, 521*, 724-736.

Alshare, A., Al-Kouz, W., & Khan, W. (2020). Cu-Al2O3 water hybrid nanofluid transport in a periodic structure. *Processes, 8*(3), 285.

Anuar, N. S., Bachok, N., & Pop, I. (2020). Cu-Al2O3/water hybrid nanofluid stagnation point flow past MHD stretching/shrinking sheet in presence of homogeneous-heterogeneous and convective boundary conditions. *Mathematics, 8*(8), 1237.

Bahiraei, M., Jamshidmofid, M., & Heshmatian, S. (2017). Entropy generation in a heat exchanger working with a biological nanofluid considering heterogeneous particle distribution. *Advanced Powder Technology, 28*(9), 2380-2392.

Barozzi, G. S., Zanchini, E., & Mariotti, M. (1985). Experimental investigation of combined forced and free convection in horizontal and inclined tubes. *Meccanica, 20*, 18-27.

Bejan, A. (2013). *Convection heat transfer*: John wiley & sons.

Bejan, A., & Kestin, J. (1983). Entropy generation through heat and fluid flow.

Bejan, A., & Lorente, S. (2012). The physics of spreading ideas. *International Journal of Heat and Mass Transfer, 55*(4), 802-807.

Bergman, T. L., Bergman, T. L., Incropera, F. P., Dewitt, D. P., & Lavine, A. S. (2011). *Fundamentals of heat and mass transfer*: John Wiley & Sons.

Bergman, T. L., Lavine, A. S., Incropera, F. P., & DeWitt, D. P. (2011). *Introduction to heat transfer*: John Wiley & Sons.

Esfahani, J., Akbarzadeh, M., Rashidi, S., Rosen, M., & Ellahi, R. (2017). Influences of wavy wall and nanoparticles on entropy generation over heat exchanger plat. *International Journal of Heat and Mass Transfer, 109*, 1162-1171.

Farouk, B., & Ball, K. S. (1985). Convective flows around a rotating isothermal cylinder. *International Journal of Heat and Mass Transfer, 28*(10), 1921-1935.

Fluent, I. (2006). FLUENT user's guide 6.3. *Lebanon, USA*.

Galvez, M., Loutzenhiser, P. G., Hischier, I., & Steinfeld, A. (2008). CO2 splitting via two-step solar thermochemical cycles with Zn/ZnO and FeO/Fe3O4 redox reactions: thermodynamic analysis. *Energy & Fuels, 22*(5), 3544-3550.

Ghadikolaei, S., Yassari, M., Sadeghi, H., Hosseinzadeh, K., & Ganji, D. (2017). Investigation on thermophysical properties of Tio2–Cu/H2O hybrid nanofluid transport dependent on shape factor in MHD stagnation point flow. *Powder Technology, 322*, 428-438.

Ghajar, A. J., & Tam, L.-M. (1995). Flow regime map for a horizontal pipe with uniform wall heat flux and three inlet configurations. *Experimental Thermal and Fluid Science, 10*(3), 287-297.

Ghasemi, B., & Aminossadati, S. (2010). Periodic natural convection in a nanofluid-filled enclosure with oscillating heat flux. *International Journal of Thermal Sciences, 49*(1), 1-9.

Hooman, K. (2006). Entropy-energy analysis of forced convection in a porous-saturated circular tube considering temperature-dependent viscosity effects. *International Journal of Exergy, 3*(4), 436-451.

Ibáñez, G., Cuevas, S., & de Haro, M. L. (2003). Minimization of entropy generation by asymmetric convective cooling. *International Journal of Heat and Mass Transfer, 46*(8), 1321-1328.

Iqbal, M., & Stachiewicz, J. (1966). Influence of tube orientation on combined free and forced laminar convection heat transfer.

Joye, D. D., Bushinsky, J. P., & Saylor, P. E. (1989). Mixed convection heat transfer at high Grashof number in a vertical tube. *Industrial & engineering chemistry research, 28*(12), 1899-1903.

Kakaç, S., Shah, R. K., & Aung, W. (1987). Handbook of single-phase convective heat transfer.

Karwe, M. V., & Deo, I. (2003). Grashof number. *Encyclopedia of agricultural, food, and biological engineering, 1*(1), 454-456.

Khfagi, A. M., Hunt, G., Paul, M. C., & Karimi, N. (2022). Computational analysis of heat transfer augmentation and thermodynamic irreversibility of hybrid nanofluids in a tube fitted with classical and elliptical-cut twisted tape inserts. *Journal of Thermal Analysis and Calorimetry*, 1-18.

Lin, W., & Lin, T. (1996). Unstable aiding and opposing mixed convection of air in a bottom-heated rectangular duct slightly inclined from the horizontal.

Mansour, R. B., Galanis, N., & Nguyen, C. T. (2007). Effect of uncertainties in physical properties on forced convection heat transfer with nanofluids. *Applied Thermal Engineering, 27*(1), 240-249.

Maughan, J., & Incropera, F. P. (1987). Experiments on mixed convection heat transfer for airflow in a horizontal and inclined channel. *International Journal of Heat and Mass Transfer, 30*(7), 1307-1318.

Mehryan, S. A., Kashkooli, F. M., Ghalambaz, M., & Chamkha, A. J. (2017). Free convection of hybrid Al2O3-Cu water nanofluid in a differentially heated porous cavity. *Advanced Powder Technology, 28*(9), 2295-2305.

Meyer, J. P., & Everts, M. (2018). Single-phase mixed convection of developing and fully developed flow in smooth horizontal circular tubes in the laminar and transitional flow regimes. *International Journal of Heat and Mass Transfer, 117*, 1251-1273.

Mirmasoumi, S., & Behzadmehr, A. (2008). Effect of nanoparticles mean diameter on mixed convection heat transfer of a nanofluid in a horizontal tube. *International journal of heat and fluid flow, 29*(2), 557-566.

Mohammed, H. A. (2008). Laminar mixed convection heat transfer in a vertical circular tube under buoyancy-assisted and opposed flows. *Energy conversion and management, 49*(8), 2006-2015.

Mwesigye, A., Bello-Ochende, T., & Meyer, J. P. (2014). Minimum entropy generation due to heat transfer and fluid friction in a parabolic trough receiver with non-uniform heat flux at different rim angles and concentration ratios. *Energy, 73*, 606-617.

Nimmagadda, R., & Venkatasubbaiah, K. (2015). Conjugate heat transfer analysis of micro-channel using novel hybrid nanofluids (Al2O3+ Ag/Water). *European Journal of Mechanics-B/Fluids, 52*, 19-27.

Oliveski, R. D. C., Macagnan, M. H., & Copetti, J. B. (2009). Entropy generation and natural convection in rectangular cavities. *Applied Thermal Engineering, 29*(8-9), 1417-1425.

Oni, T. O., & Paul, M. C. (2014). Numerical simulation of turbulent heat transfer and fluid flow in different tube designs.

Oni, T. O., & Paul, M. C. (2015). Assessment of mixed convection heat transfer in a flow through an induced tube. *International Invention Journal of Engineering Science and Technology, 2*, 17-30.

Oni, T. O., & Paul, M. C. (2016). Numerical investigation of heat transfer and fluid flow of water through a circular tube induced with divers' tape inserts. *Applied Thermal Engineering, 98*, 157-168.

Ozsunar, A., Baskaya, S., & Sivrioglu, M. (2001). Numerical analysis of Grashof number, Reynolds number and inclination effects on mixed convection heat transfer in rectangular channels. *International Communications in Heat and Mass Transfer, 28*(7), 985-994.

Paoletti, S., Rispoli, F., & Sciubba, E. (1989). *Calculation of exergetic losses in compact heat exchanger passages.* Paper presented at the Asme Aes.

Patankar, S. V., & Spalding, D. B. (1983). A calculation procedure for heat, mass and momentum transfer in three-dimensional parabolic flows. In *Numerical prediction of flow, heat transfer, turbulence and combustion* (pp. 54-73): Elsevier.

Patil, S., & Vijay Babu, P. (2012). Experimental studies on mixed convection heat transfer in laminar flow through a plain square duct. *Heat and mass transfer, 48*(12), 2013-2021.

Piva, S., Barozzi, G. S., & Collins, M. (1995). Combined convection and wall conduction effects in laminar pipe flow: numerical predictions and experimental validation under uniform wall heating. *Heat and mass transfer, 30*(6), 401-409.

Polidori, G., Fohanno, S., & Nguyen, C. (2007). A note on heat transfer modelling of Newtonian nanofluids in laminar free convection. *International Journal of Thermal Sciences, 46*(8), 739-744.

Qureshi, M. A., Hussain, S., & Sadiq, M. A. (2021). Numerical simulations of MHD mixed convection of hybrid nanofluid flow in a horizontal channel with cavity: Impact on heat transfer and hydrodynamic forces. *Case Studies in Thermal Engineering, 27*, 101321.

Rahmati, A. R., Roknabadi, A. R., & Abbaszadeh, M. (2016). Numerical simulation of mixed convection heat transfer of nanofluid in a double lid-driven cavity using lattice Boltzmann method. *Alexandria Engineering Journal, 55*(4), 3101-3114.

Rashidi, M. M., Nasiri, M., Khezerloo, M., & Laraqi, N. (2016). Numerical investigation of magnetic field effect on mixed convection heat transfer of nanofluid in a channel with sinusoidal walls. *Journal of Magnetism and Magnetic Materials, 401*, 159-168.

Saysroy, A., & Eiamsa-ard, S. (2017). Periodically fully-developed heat and fluid flow behaviors in a turbulent tube flow with square-cut twisted tape inserts. *Applied Thermal Engineering, 112*, 895-910.

Shahsavar, A., Moradi, M., & Bahiraei, M. (2018). Heat transfer and entropy generation optimization for flow of a non-Newtonian hybrid nanofluid containing coated CNT/Fe3O4 nanoparticles in a concentric annulus. *Journal of the Taiwan Institute of Chemical Engineers, 84*, 28-40.

Sheikholeslami, M., Jafaryar, M., & Li, Z. (2018). Second law analysis for nanofluid turbulent flow inside a circular duct in presence of twisted tape turbulators. *Journal of Molecular Liquids, 263*, 489-500. doi:10.1016/j.molliq.2018.04.147

Shih, T.-H. (1993). *A realizable Reynolds stress algebraic equation model* (Vol. 105993): Lewis Research Center, Institute for Computational Mechanics in Propulsion.

Singh, P. K., Anoop, K., Sundararajan, T., & Das, S. K. (2010). Entropy generation due to flow and heat transfer in nanofluids. *International Journal of Heat and Mass Transfer, 53*(21-22), 4757-4767.

Taher, R., Ahmed, M. M., Haddad, Z., & Abid, C. (2021). Poiseuille-Rayleigh-Bénard mixed convection flow in a channel: Heat transfer and fluid flow patterns. *International Journal of Heat and Mass Transfer, 180*, 121745.

Takabi, B., & Salehi, S. (2014). Augmentation of the heat transfer performance of a sinusoidal corrugated enclosure by employing hybrid nanofluid. *Advances in Mechanical Engineering, 6*, 147059.

Vajjha, R. S., & Das, D. K. (2008). *Measurements of specific heat and density of Al 2 O 3 nanofluid.* Paper presented at the AIP Conference Proceedings.

Varol, Y., Oztop, H. F., & Koca, A. (2008). Entropy production due to free convection in partially heated isosceles triangular enclosures. *Applied Thermal Engineering, 28*(11-12), 1502-1513.

Versteeg, H. K., & Malalasekera, W. (2007). *An introduction to computational fluid dynamics: the finite volume method*: Pearson education.

Yan, W.-M. (1994). Mixed convection heat and mass transfer in inclined rectangular ducts. *International Journal of Heat and Mass Transfer, 37*(13), 1857-1866.

Zadeh, S. M. H., Mehryan, S., Islam, M. S., & Ghalambaz, M. (2020). Irreversibility analysis of thermally driven flow of a water-based suspension with dispersed nano-sized capsules of phase change material. *International Journal of Heat and Mass Transfer, 155*, 119796.

Zimparov, V. (2001). Extended performance evaluation criteria for enhanced heat transfer surfaces: heat transfer through ducts with constant heat flux. *International Journal of Heat and Mass Transfer, 44*(1), 169-180. doi:10.1016/s0017-9310(00)00074-0